J IRAN CHEM SOC (2016) 13:1429–1437
DOI 10.1007/s13738-016-0858-2

ORIGINAL PAPER

# Flubendazole Pd(II) complexes: structural studies, cytotoxicity, and quantum chemical calculations

**Ahmed M. Mansour[1] · Eslam M. El Bakry[1] · Nour T. Abdel-Ghani[1]**

Received: 27 December 2015 / Accepted: 9 April 2016 / Published online: 23 April 2016


**Abstract** $[Pd(FLU)_2X_2]\cdot yH_2O\cdot zCH_3OH$ (FLU = flubendazole; X = Cl (**1**), $y = 0$, $z = 0$; X = Br (**2**), $NO_3$ (**3**), $y = 2$, $z = 0$; X = SCN (**4**), $y = 2$, $z = 3$) were synthesized as potential anticancer complexes, and their structures were elucidated using elemental analysis, TG/DTA, IR, $^1$H NMR, UV–vis., and conductivity measurements. FLU interacts with Pd(II) ions as a neutral unidentate ligand via the pyridine-type nitrogen of the benzimidazole ring. Geometry optimization, molecular electrostatic potential maps and natural bond orbital analysis were performed by DFT/B3LYP method. FLU, in comparison to its complexes, was screened for its antibacterial and cytotoxic activity. Complexes **1–4** possess strong anticancer activity with $IC_{50}$ values (4.13–3.68 μg ml$^{-1}$) compared with 3.57 μg ml$^{-1}$ reported for cis-platin. The cytotoxicity was shown to be affected by the nature of the anion, where the sequence is **3 > 2 > 4 > 1** in case of MCF7 cell line. Structural-activity relationships suggested that $E_{HOMO}$, energy gap and dipole moment were the most significant descriptors for the correlation with the antitumor activity.

**Keywords** Flubendazole · DFT · Biological activity · NMR · NBO · B3LYP

**Electronic supplementary material** The online version of this article (doi:10.1007/s13738-016-0858-2) contains supplementary material, which is available to authorized users.

✉ Ahmed M. Mansour
mansour@sci.cu.edu.eg; inorganic_am@yahoo.com

✉ Nour T. Abdel-Ghani
noureta2002@yahoo.com

[1] Chemistry Department, Faculty of Science, Cairo University, Gamaa Street, Giza 12613, Egypt

## Introduction

The benzimidazole scaffold is a useful structural motif for displaying the chemical functionality in the biologically active molecules. Some of its derivatives have potent biological activities as antitumor, anti-HIV, and antimicrobial agents [1–4]. 5,6-Dimethylbenzimidazole is present in vitamin $B_{12}$ and other related biomolecules [5]. Besides, benzimidazoles were used also in liquid crystals [6], OLED's [7–9], switch's devices [10], DNA intercalator [2, 11] and corrosion inhibitors [12]. At the same time, owing to the coordination ability of azoles, the benzimidazole chelating ligands have been extensively studied in the modeling biological systems [13, 14]. Benzimidazole can act as a monodentate ligand or as bridge forming a variety of the polynuclear complexes [15] of intriguing research applications. A considerable number of metal complexes including Cr–Zn, Pd, Pt, Au and Re was studied [15–23], and subjected to different applications [24, 25]. Flubendazole (FLU, Scheme 1) is a benzimidazole carbamate used for the treatment of the cystic echinococcosis in animals [26, 27] and humans [28, 29] causing significant in vitro damage on the protoscoleces and cysts of *Echinococcus granulosus*. FLU is more effective than the other carbamates in the treatment of the resistant strains of *Haemonchus contortus* and *Schistosoma mansoni* infected mice [30]. Its anthelmintic activity against *Toxocara canis* [31], *Trichuris trichiura*, *Ascaris lumbricoides, Onchocerca ochengi*, *Ascaridia galli*, *Heterakis gallinarum* and *intestinal Capillaria* spp. [32, 33] has been also reported. Several analytical techniques [34–36] were used for the determination of FLU in its pure form and pharmaceutical preparations. The identification of the metabolic pathways of FLU in helminthes parasites was also studied [37].

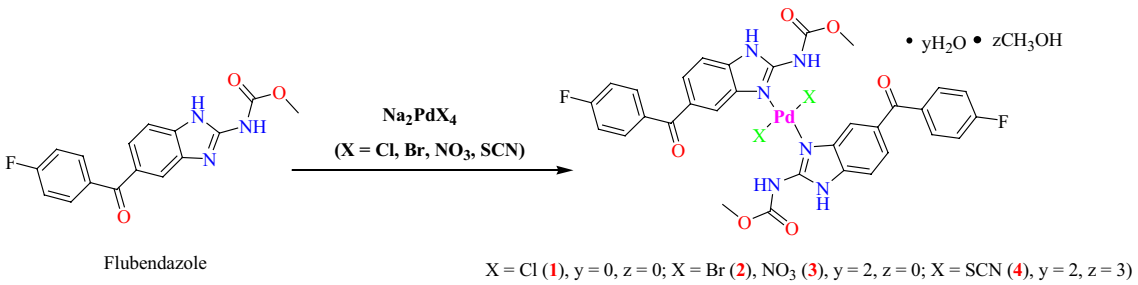


**Scheme 1** Synthesis of the investigated Pd(II)–flubendazole complexes

In this study, our aim was to take into account all the previously mentioned properties of anticancer drugs and synthesize new Pd(II) complexes of FLU that could prove to be potent antitumor agents. Structural characterizations are reported both experimentally and theoretically using several analytical and spectral methods. The synthesized compounds have been screened for their antitumor activity on *human breast cancer*, *hepatocarcinoma* and colon *carcinoma cells* cell lines and against some microorganisms for their antimicrobial activity.

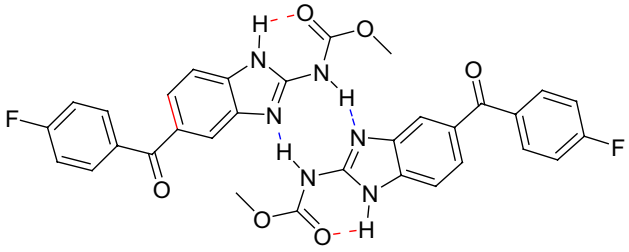

**Fig. 1** Inter- and intramolecular hydrogen bonds stabilizing the crystal packing of FLU

## Results and discussion

### Structural characterization

The solid Pd(II) complexes of FLU [X = Cl (**1**), Br (**2**), $NO_3$ (**3**) and SCN (**4**)] were synthesized as shown in (Scheme 1). The complexes were characterized by elemental analysis, TG/DTA, IR, $^1$H NMR, UV–Vis and conductance measurements. The IR spectrum of FLU showed a broad band in 3500–2200 $cm^{-1}$ range arising from $C{=}N_{Bz}{\ldots}NH_{carb}$ (Bz: benzimidazole, carb: carbamate) [38] and $C{=}O_{carb}{\ldots}NH_{Bz}$ interactions (Fig. 1). Therefore, it was not easy to assign $\nu(NH_{Bz})$ [16–18]. The coordination of FLU to Pd(II) ion via the benzimidazole ring inhibits the inter-H-bond contacts, and gives rise to a sharp band in 3308–3271 $cm^{-1}$. FLU is characterized by sharp bands at 3308, 1735 and 1646 $cm^{-1}$ allocated to $\nu(NH_{carb})$, $\nu(C{=}O_{carb})$, and $\nu(C{=}O_{benzoyl})$ in that order. In complexes, these modes are shifted to higher values, 3387–3475, 1745–1735 and 1646–1648 $cm^{-1}$ excluding the participation of these groups in the coordination spheres [39]. Owing to the effect of H-bonds, the $\nu(C{=}N) + \nu(C{=}C)$ combination in the free FLU was observed at lower wave number, 1595 $cm^{-1}$. Upon complex formation, the effect of H-bond on $C{=}N_{Bz}$ group is replaced by the complex formation with a slightly shift in its vibration. The $\nu(C{=}N)$ was found at 1590 for (**1**) and 1592 $cm^{-1}$ for (**2**), while it is still overlapped in **3** and **4**. The IR spectrum of **3** displays two new bands at 1356 and 1275 $cm^{-1}$, assigned to the N–O stretching vibration $\nu_3(NO_3)$ modes [40, 41]. Small splitting of $\nu_3(NO_3)$ bands ($\Delta(\nu_3) < 120$ $cm^{-1}$) confirms the presence of a monodentate nitrate group. Complex **4** shows also a new band at 2160 $cm^{-1}$ assigned to $\nu(C{\equiv}N)$ of the SCN groups. The relatively high wave number value suggests the formation of Pd–S rather than Pd–N [42].

The $^1$H NMR spectrum of FLU exhibits two singlet signals at 11.89 ($NH_{Bz}$) and 6.66 ppm ($NH_{carb}$). The signal of $–CH_3$ is observed at 3.83 ppm, while the benzimidazole signals are shown at 7.42, 7.85 and 7.86. The benzoyl ring protons display four-line pattern at 7.22 and 7.25 ppm for the two protons adjacent to C=O and 7.58 and 7.59 ppm to the others. In complexes, the $NH_{Bz}$ was observed in the 11.80–12.50 ppm range, which can be related to the charge density change in the benzimidazole ring supporting the coordination via the pyridine-type nitrogen [16–18, 43]. The signal of $NH_{carb}$ is slightly shifted down field, to be obscured by the aromatic signals except **3** (6.80 ppm). This may be attributed to the involvement of the $NH_{carb}$ group in H-bonds with the coordinated nitrate groups (discussed later). For complex **4**, the methanol signals were found at 2.55 ($CH_3$) and 3.22 ppm (OH).

The thermal decomposition of **1** exhibits two endothermic peaks at 270 and 410 °C assigned to loss of 2Cl + one $OCH_3$ group (observed mass loss 13.10 %, calcd. 12.68 %), and the rest of the organic part, respectively, leaving Pd metal contaminated with carbon as a final residue with overall mass loss amounts to 80.22 % (calcd. 80.79 %).

Complex **2** decomposes in four endothermic steps at 36, 236, 297 and 494 °C. The 1st step is responsible for desorption of $2H_2O$ (observed 4.17 %, calcd. 3.88 %). The elimination of 2Br via the 2nd and 3rd stages brings the mass loss to 17.33 % (calcd. 17.20 %). The 4th stage may be assigned to pyrolysis of two FLU molecules giving Pd + 2C as a final residue (total mass loss observed 85.31 %, calcd. 85.96 %) [44]. The TG/DTA curves of **3** show two endothermic steps at 231 and 358 °C. The 1st step with a mass loss of 11.11 % (calcd. 10.98 %) is due to the loss of two lattice $H_2O$ molecules, and one $NO_3$ group. The thermal degradation of **3** is incomplete up to 1000 °C [45]. The overall mass loss amounts to 77.79 % (calcd. 88.08 %) assuming the formation of Pd metal as a final residue as no Pd compounds are present at 1000 °C. For **4**, four decomposition stages at 237, 326, 413 and 414 °C were reported. The 1st stage was assigned to the elimination of $3CH_3OH + 2H_2O$ (observed mass loss 13.78 %, calcd. 13.46 %). The degradation of two FLU molecules and two SCN groups proceeds through three overlapped decomposition stages with a total mass loss of 89.44 % (calcd. 89.15 %) leaving elemental Pd as a final residue.

## Electronic structure

The electronic absorption spectrum of FLU in DMF displays two bands at 267 and 319 nm assigned to the $\pi$–$\pi^*$ transition of the benzimidazole ring [43] and $n$–$\pi^*$ transition of the C=O groups in that order. The characteristic fine structure of benzimidazole ring [45] is not present confirming the participation of $NH_{Bz}$ in the intra-H-bond. The nature of the bands has been established by observing the absorption spectra of FLU in solvents of different polarity and H-bond formation tendency (Fig. S1†); $CHCl_3$, DMSO, $CCl_4$, ethanol and dioxane. The values of $\lambda_{max}$, $\varepsilon_{max}$, observed transition energies ($E_{obs}$) and oscillator strengths ($f_{obs}$) of the bands are presented in Table S1†. The bands at 267 and 319 nm in DMF are blue shifted to 255 and 312 nm in ethanol (H-bonding solvent) suggesting that FLU is acting as a proton acceptor at pyridine-type nitrogen ($N_{py}$). The pH dependency of the absorption spectra of FLU in 30 % aqueous/DMF was investigated in the pH = 2–12 range (Fig. 2). Two isosbestic points, in the acidic medium (pH = 2.98–4.23) at 265 and 305 nm were observed corresponding to the equilibrium between the monocation-neutral species as a result of the protonation of $N_{py}$ [46]. In the pH range of 4.23–8.29, FLU remains unaffected by change of pH. In the alkaline medium, two new isosbestic points were found at 290 and 330 nm assigned to the ionization of two NH protons. Three p$K_a$ values were reported for FLU at 3.28 ± 0.029, 8.28 ± 0.039 and 9.64 ± 0.082 assigned to deprotonation of the protonated $NH_{carb}$, ionization of $NH_{carb}$, and $NH_{Bz}$, respectively.

The electronic spectra of **1**–**4** exhibit two bands at 260 and 275 nm assigned to the internal ligand transitions. To get deep understandings of the transitions occurring in the complexes, TD-DFT calculations were performed. The calculated spectrum of **1** in DMSO shows two transitions at 322 and 448 (shoulder) nm assigned mainly to H → L+2 and H-1/H-14 → L (H: HOMO and L: LUMO) in that order. Similar, two bands were calculated in **2** at 322 and 440 nm with oscillator strengths 0.3301 and 0.0032, respectively. These bands are allocated to H → L + 1 and H-2/H-16 → L as shown in Fig. 3. Complex **3** displays two

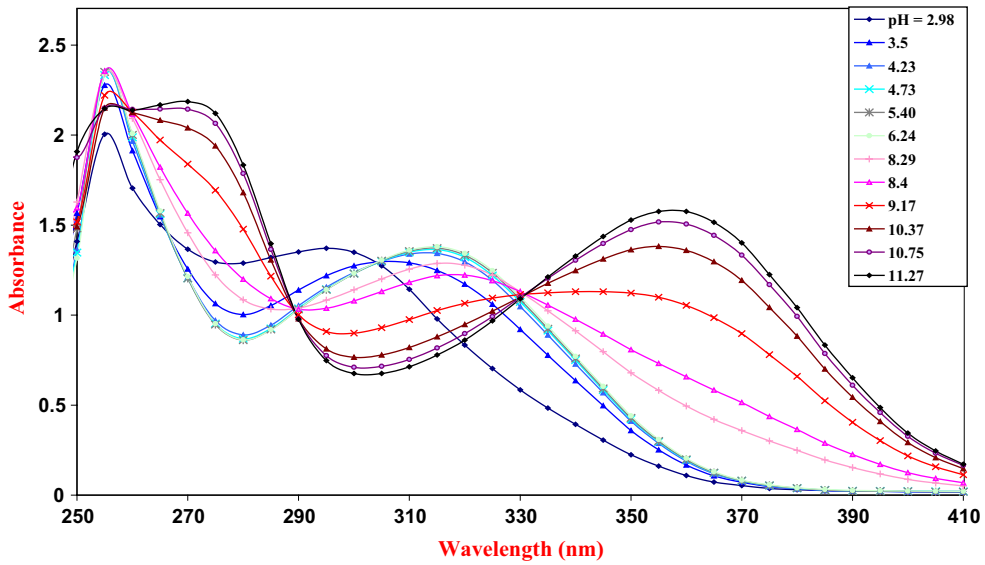


**Fig. 2** Electronic absorption spectra of FLU in solutions of varying pH

bands at 316 and 419 nm with oscillator strengths 0.6855 and 0.0052. The electronic transition (Fig. S2†) at 316 nm is arising from the H-1 → L+3 and H → L + 4 transitions, while the band at 419 nm characterizes H-1 → L. The TD-DFT spectrum of **4** shows two main transitions at 510 and 463 nm allocated for H → L, and H-6 → L, respectively.

## DFT studies

A view of the optimized FLU structure and its atoms numbering is displayed (Fig. S3†). Selected bond distances are listed in Table S2†. The optimized geometry was compared with the crystallographic data of those closely related molecules, Mebendazole [38] and 2-methyl benzimidazole carbamate [47]. Most of the bond lengths are in agreement with the crystal data of Mebendazole within |0.000–0.025| Å except C4–C5 (0.036 Å), N11–C12 (0.036 Å), C1–N10 (0.035 Å), N13–C15 (0.035 Å), N10–C12 (0.067 Å), and C26–C30 (0.043 Å). The minor discrepancy may be justified on the basis that the calculations were performed on a single molecule in the gaseous state contrary to the experimental values, which were recorded in the solid state. A slight disagreement in N10–C12 and C1–N10 bond lengths on one hand, and N13–C15, and N11–C12 on the other hand may be attributed to the intra- and inter-hydrogen bonds. The standard deviation in the bond lengths was found to be 0.011 Å for Mebendazole and 0.023 Å for 2-methyl benzimidazole carbamate.

A view of the optimized structures of **1** and **2** and their atom numbering are shown in Fig. 4. Selected bond distances and angles are listed in Table S3†. The square planar geometries of **1** and **2** are formed by $N_{py}$ atoms of two monodentate FLU molecules [Pd–N1 = Pd–N2 = 2.062 Å (**1**) and Pd–N1 = Pd–N2 = 2.061 Å (**2**)], two Cl/Br atoms [PdCl(72) = PdCl(73) = 2.424 Å and PdBr(72) = PdBr(73) = 2.568 Å] in a trans arrangement. Two intra H-bonds affecting the length of Pd-X were observed. For example, the Cl…H–N interaction (2.296 Å) in **1** is stronger than Br…H–N for **2** (2.576 Å), since the

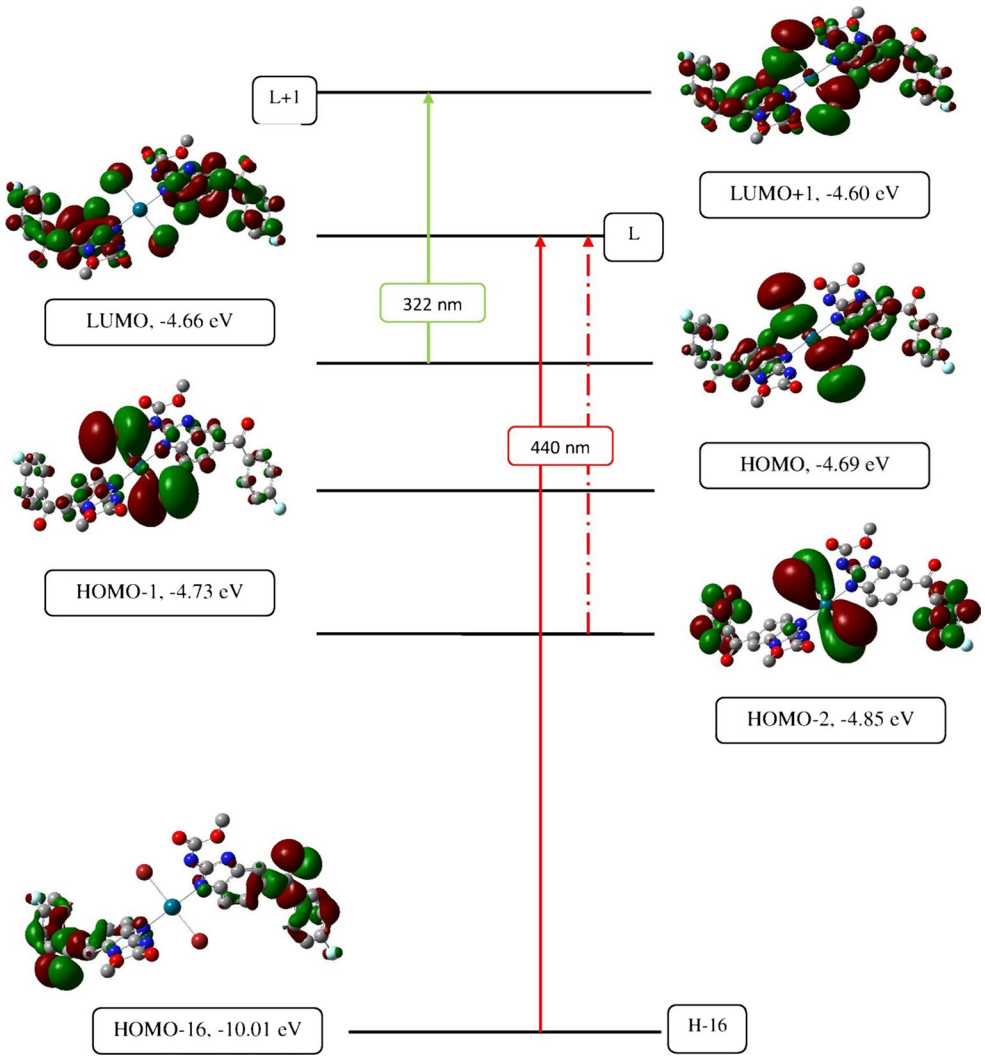


**Fig. 3** Theoretical electronic absorption transitions of complex **2** in DMSO

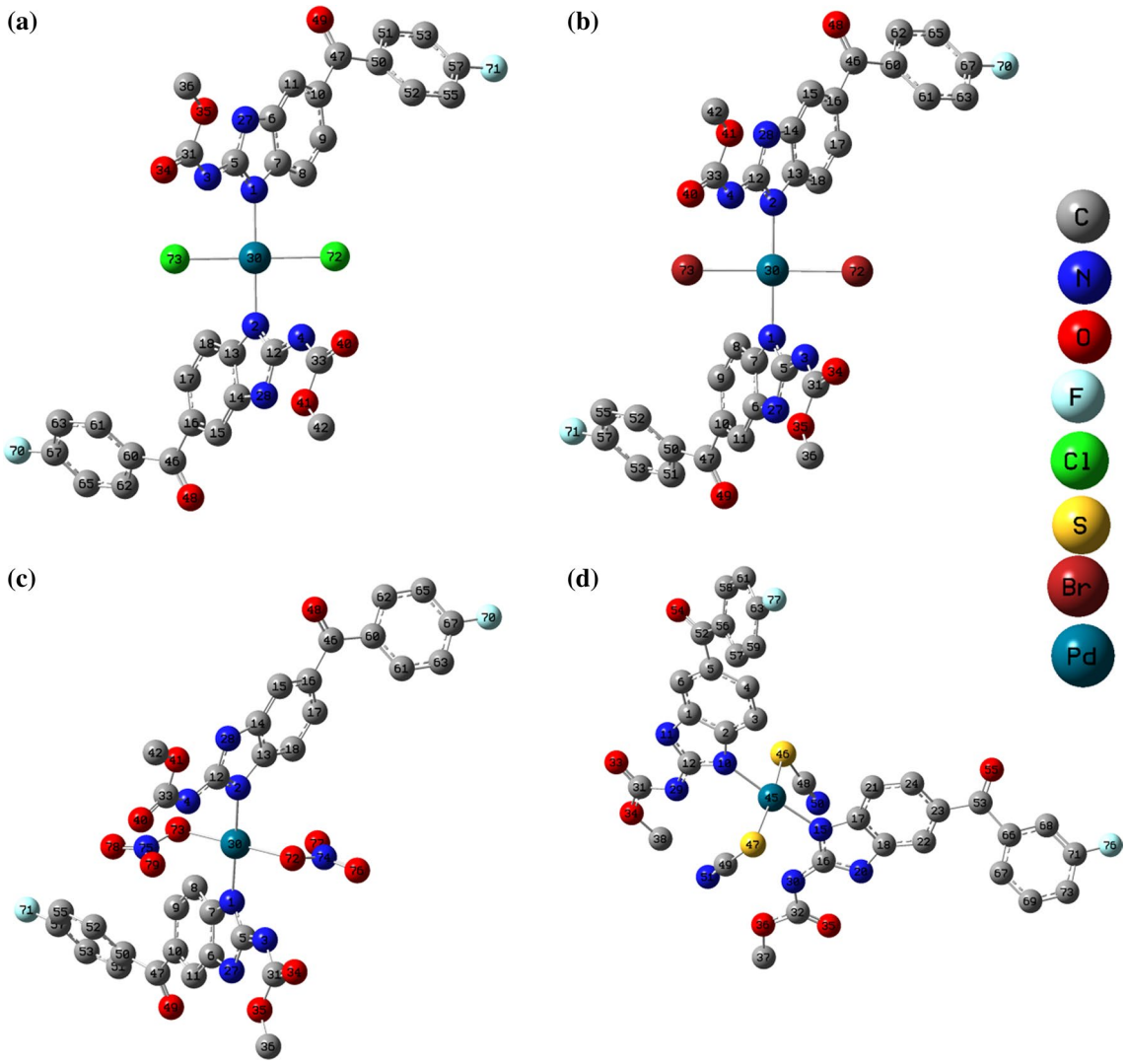


**Fig. 4** Local minimum structures of complexes (**a**) **1**, (**b**) **2**, (**c**) **3**, and (**d**) **4** obtained at the DFT/B3LYP level of theory

**Table 1** Electronic configuration, *d*-subshell populations and charge of the Pd atom in the studied complexes

| Complex | Electronic arrangement | $d_{xy}$ | $d_{xz}$ | $d_{yz}$ | $d_{x^2-y^2}$ | $d_{z^2}$ | Charge on Pd |
|---|---|---|---|---|---|---|---|
| **1** | $[Kr]5s^{0.36}4d^{8.92}5p^{0.20}6p^{0.16}$ | 1.98569 | 1.20920 | 1.99278 | 1.86028 | 1.86729 | 0.36373 |
| **2** | $[Kr]5s^{0.39}4d^{8.98}5p^{0.22}5d^{0.01}6p^{0.19}$ | 1.98595 | 1.35528 | 1.99389 | 1.81554 | 1.83080 | 0.22554 |
| **3** | $[Kr]5s^{0.30}4d^{8.77}5p^{0.25}5d^{0.01}$ | 1.95874 | 1.26452 | 1.89102 | 1.84442 | 1.81479 | 0.67793 |
| **4** | $[Kr]5s^{0.38}4d^{9.03}5p^{0.37}5d^{0.01}$ | 1.96028 | 1.94948 | 1.98926 | 1.69060 | 1.43641 | 0.22982 |

angle of the former interaction approaches more linearity [39]. According to natural bond orbital (NBO) analysis [48, 49], the natural charge on the Pd metal center is reduced significantly from the formal charge +2 as a consequence of electron density donation from the coordination sphere active centers. The electronic configuration of Pd in **1** is $[Kr]5s^{0.36}4d^{8.92}5p^{0.20}6p^{0.16}$ with 9.772 valence electrons giving total 45.636 electrons and leaving +0.364e as a natural charge. The 4d orbitals are occupied as tabulated in Table 1. Comparison between **1** and **2** showed that the distribution of electrons between the highest square planar orbitals ($d_{x^2-y^2} > d_{xy} > d_{z^2} > d_{xz}/d_{yz}$) is different.

The geometries of **3** and **4** (Fig. 4) are formed by $N_{py}$ atoms of two FLU [PdN1 = 2.085, PdN2 = 2.068 Å for **3** and Pd–N10 = 2.073 Å, Pd–N15 = 2.064 Å for **4**], and two oxygen atoms of two monodentate $NO_3^-$ [PdO72 = PdO73 = 2.043

**Table 2** Second-order interaction energy ($E^2$, kcal/mol) between donor and acceptor orbitals in the studied complexes calculated at B3LYP/LANL2DZ level of theory (selected)

| Donor → acceptor | $E^2$ | Donor → acceptor | $E^2$ |
|---|---|---|---|
| **1** | | | |
| LP(4)Cl (1) → RY*(9)Pd | 1.79 | LP(1)N3 → RY*(9)Pd | 1.42 |
| LP(1)N2 → RY*(9)Pd | 1.42 | LP(4)Cl (35) → RY*(9)Pd | 1.79 |
| **2** | | | |
| LP(1)N1 → RY*(4)Pd | 1.10 | LP(4)Br72 → RY*(4)Pd | 0.98 |
| LP(1)N2 → RY*(4)Pd | 1.10 | LP(4)Br73 → RY*(4)Pd | 0.98 |
| **3** | | | |
| LP(1)N1 → RY*(8)Pd | 1.41 | LP(3)O72 → RY*(8)Pd | 0.87 |
| LP(1)N2 → RY*(8)Pd | 1.64 | LP(3)O73 → RY*(8)Pd | 0.68 |
| **4** | | | |
| LP(1)N10 → RY*(9)Pd | 0.31 | LP(3)S46 → RY*(9)Pd | 1.38 |
| LP(1)N15 → RY*(9)Pd | 0.34 | LP(1)S47 → σ*Pd–S47 | 0.29 |

Å] in **3** or two SCN groups [PdS46 = 2.396 Å and PdS47 = 2.468 Å] in **4**. The inequality in Pd–S bond is attributed to the involvement of SCN group in H-bonds with carbamate NH groups [N51…H28N30 = 2.284 Å, and N51…H14N29 = 2.359 Å] and methyl group [N51…H39C38 = 2.401 Å]. The electronic arrangement of Pd in **3** is $[Kr]5s^{0.30}4d^{8.77}5p^{0.25}5d^{0.01}$, with 36 core electrons, 9.321 valence electrons, and 0.01121 Rydberg electrons, which gives 45.322 total electrons and +0.678e charge on the central atom. The natural charge of Pd in **4** is similar to **2**, but is more reduced than those of **1** and **3** suggesting the presence of strong interaction and electron donation from the SCN groups to the metal center. The 4d-subshell electrons (9.03e) are distributed as $d_{xy}^{1.960}\ d_{xz}^{1.949}\ d_{yz}^{1.989}\ d_{x^2-y^2}^{1.690}\ d_{z^2}^{1.436}$. The strength of interaction between the metal center and active binding sites was assigned by the second order interaction energy ($E^2$) [16–18]. Table 2 lists the selected values of the $E^2$ values between donor–acceptor orbitals in the studied complex. For **1** and **2**, the interactions between the FLU molecules and Pd are equal indicating the isoenergetical existence of the two ligands. These M–L interactions are not equal in case of **3** and **4** suggesting the effect of the $NO_3$ and SCN in making the two ligands nonequivalent.

## Biological activity

### *Antimicrobial activity*

FLU and its complexes were screened in vitro for their antibacterial activity against culture of *S. aureus* ($G^+$), and *E. coli* ($G^-$) and compared to tetracycline used as a standard. The tested compounds are inactive against the tested microorganisms.

### *Anticancer activity*

To evaluate the potential usefulness of the Pd(II) complexes synthesized as antitumor agents, three cell lines of different origin *breast cancer* (MCF7), *colon carcinoma* (HCT) and *human hepatocarcinoma* ($HepG_2$) were treated (Table S4†). In the preliminary assay, the studied compounds were tested for their cytotoxic activities at concentration of 100 μg $ml^{-1}$. The $IC_{50}$ (the concentration that inhibited in 50 % of the cellular proliferation) of the complexes and cisplatin were determined and compared with cis-platin (Fig. S4†). According to Shier [50], the compounds exhibited $IC_{50}$ activity within the range of 10–25 μg $ml^{-1}$ are considered weak anticancer drugs, while those of $IC_{50}$ activity between 5 and 10 μg $ml^{-1}$ are moderate and compounds of activity below 5 μg $ml^{-1}$ are considered strong antitumour agents. On screening against MCF7, it was found that complexes **1–4** possess strong anticancer activity with $IC_{50}$ values of 4.13, 3.53, 3.68, and 3.68 μg $ml^{-1}$, respectively (equivalent to 5.13, 3.80, 3.96, and 3.75 μM) comparing with 3.57 μg $ml^{-1}$ (11.90 μM), for cis-platin. The inhibitory activity of **1–4** are shown to be affected by the nature of the anion, where the sequence follows the order $NO_3$(**3**) > Br(**2**) > SCN(**4**) > Cl(**1**). In case of $HepG_2$ cell line, the cytotoxicity of **1–4** decreases in the following arrange **2** > **3** > **1** > **4**. On the other hand, complex **1** has the highest activity against HCT, while compound **2** has the lowest toxicity.

## Structure–activity relationship (SAR)

The decisive aim of SAR studies [51] is to correlate the antitumor activity of complexes **1–4** with some appropriate quantum chemical descriptors based on DFT calculations (Table S5†). $E_{HOMO}$ indicates the ability of the molecule to donate electrons, while $E_{LUMO}$ is associated with the electron accepting ability. A good correlation ($R^2$ = 0.9109) was set up between the experimental $IC_{50}$ values (against MCF7) and $E_{HOMO}$, where the toxicity of **2–4** decreases as $E_{HOMO}$ raises. Alternatively, the energy gap decides whether the molecule is hard or soft [49]. Complex **3** was harder than the other complexes with a highest $\Delta E$ value and lowest activity. Dipole moment was used to qualitatively analyze the trend in the hydrophobic values. Herein, the highest dipole moment value of **4** (3.75 μM) should be a considerable factor for its highest cytotoxicity. Molecular electrostatic potential (MEP) map is a very useful descriptor in understanding sites for electrophilic attack, nucleophilic reactions and hydrogen bonding interactions [52]. As shown (Fig. S5†), the main contribution to the strong positive charge region in the complexes is coming from the metal center, which can act as a site of nucleophilic attack. Alternatively, the benzoyl moieties represent the most

electronegative region and may probably show an electrophilic activity. There is also a region of zero potential spreading all over the remaining area. The theoretical analysis of some electronic properties such as electrophilicity index, electronegativity, $E_{LUMO}$, hardness and MEP maps showed no clear direct correlation with the $IC_{50}$ values.

## Conclusion

New Pd(II) complexes of flubendazole have been synthesized, characterized, and tested for their cytotoxicity against breast cancer, colon carcinoma and human hepatocarcinoma. Changing the nature of the coordinated anion X (X = Cl, Br, SCN, and $NO_3$) led to a variation in the cytotoxic activity. For example, the inhibitory activity was found to follow the order $NO_3$ > Br > SCN > Cl in case of MCF7. Structural activity relationships suggested that $E_{HOMO}$, energy gap and dipole moment were the most significant descriptors for the correlation with the antitumor activity.

## Experimental

### Synthesis of complexes

Complex **1** was prepared by suspend one mmol of FLU (313 mg) in 20 ml hot methanol and then mixed with a hot aqueous solution (60 °C) of $Na_2PdCl_4$ (1 mmol, 294.2 mg), whereupon the complex was precipitated. Complexes **2–4** were synthesized by mixing aqueous solution containing one mmol of $Na_2PdX_4$ (X = Br, $NO_3$ or SCN), which were prepared by adding 1 mmol of $Na_2PdCl_4$ to NaX or $NH_4X$ (4 mmol), with one mmol of suspended FLU in methanol. The resulting mixtures were refluxed for about 6 h, whereupon the complexes were precipitated. The low molar conductance values (9.21–46.10) indicate the non-electrolytic nature of the investigated complexes. The purity of the investigated compounds has been checked by thin-layer chromatography as a secondary determinant of purity.

- FLU ($C_{16}H_{12}FN_3O_3$). FT IR (KBr, $cm^{-1}$): 3308 $\nu(NH)_{carb}$, 1736 $\nu(C{=}O)_{carb}$, 1647 $\nu(C{=}O)_{benzoyl}$, 1595 $\nu(C{=}N) + \nu(C{=}C)$. $^1H$ NMR (DMSO-$d_6$, $\delta$, ppm): 11.89 ($NH_{Bz}$, s, 1H), 7.42, 7.86, 7.85 ($CH_{Bz}$, m, 3H), 7.59, 7.58, 7.25, 7.22 ($CH_{benzoyl}$, dd, 4H), 6.66 ($NH_{carb}$, s, 1H), 3.83 ($CH_3$, s, 3H). UV–Vis (DMF, $10^{-4}$, nm): 267, 319.
- **1**: Color: yellow. Elemental analysis (%): calcd. $C_{32}H_{24}Cl_2F_2N_6O_6$ Pd: C 47.77, H 2.99, N 10.45, found C 48.15, H 2.74, N 10.96. FT IR ($cm^{-1}$): 3437 $\nu(NH)_{carb}$, 3271 $\nu(NH)_{Bz}$, 1745 $\nu(C{=}O)_{carb}$, 1646 $\nu(C{=}O)_{benzoyl}$, 1590 $\nu(C{=}N)$. $^1H$ NMR (DMSO-$d_6$, $\delta$, ppm): 12.3 $(NH)_{Bz}$, 7.44, 7.87, 7.86 ($CH_{Bz}$, m, 3H), 7.61, 7.60, 7.35, 7.32 ($CH_{benzoyl}$, dd, 4H), 3.76 ($CH_3$, s, 3H). UV–Vis. (DMF, $10^{-4}$, nm): 270, 318. Molar cond. ($10^{-3}$ M, DMF, $\Omega^{-1}$ $cm^2$ $mol^{-1}$): 13.47.
- **2**: Color: brown. Elemental analysis (%): calcd. $C_{32}H_{28}Br_2F_2N_6O_8Pd$: C 41.35, H 3.01, N 9.04, found: C 41.23, H 3.07, N 9.13. FT IR ($cm^{-1}$): 3292 $\nu(NH)_{Bz}$, 3475 $\nu(NH)_{carb}$, 2953 $\nu(C{-}H)_{Aliph}$, 1745 $\nu(C{=}O)_{carb}$, 1646 $\nu(C{=}O)_{benzoyl}$, 1592 $\nu(C{=}N)$. $^1H$ NMR (DMSO-$d_6$, $\delta$, ppm): 12.3 $(NH)_{Bz}$, 7.44, 7.88, 7.86 ($CH_{Bz}$, m, 3H), 7.61, 7.54, 7.34, 7.31 ($CH_{benzoyl}$, dd, 4H), 3.89 ($CH_3$, s, 3H). UV–Vis (DMF, $10^{-4}$, nm): 271, 321. Molar cond. (DMF, $10^{-3}$ M, $\Omega^{-1}$ $cm^2$ $mol^{-1}$): 9.21.
- **3**: Color: dark brown. Elemental analysis (%): calcd. $C_{32}H_{28}F_2N_8O_{14}Pd$: C 43.03, H 3.14, N 12.55, found: C 43.53, H 3.11, N 11.66. FT IR ($cm^{-1}$): 3308 $\nu(NH)_{Bz,}$ 3408 $\nu(NH)_{carb}$, 2950 $\nu(C{-}H)_{aliph}$, 1737 $\nu(C{=}O)_{carb}$, 1648 $\nu(C{=}O)_{benzoyl}$, 1595 $\nu(C{=}N)$, (1356, 1275, 1202, 548, 408) $\nu(NO_3)$. $^1H$ NMR (DMSO-$d_6$, $\delta$, ppm): 12.50 $(NH)_{Bz}$, 7.42, 7.86, 7.84 ($CH_{Bz}$, m, 3H), 7.62, 7.60, 7.27, 7.25 ($CH_{benzoyl}$, dd, 4H), 6.8 ($NH_{carb}$, s, 1H), 3.89 ($CH_3$, s, 3H). UV–Vis (DMF, $10^{-4}$, nm): 260, 270, 322. Molar cond. (DMF, $10^{-3}$ M, $\Omega^{-1}$ $cm^2$ $mol^{-1}$): 10.53.
- **4**: Color: pale yellow. Elemental analysis (%): calcd. $C_{37}H_{40}F_2N_8O_{11}S_2Pd$: C 45.36, H 4.09, N 11.42, found: C 45.26, H 4.19, N 12.92. FT IR: 3308 $\nu(NH)_{Bz}$, 3387 $\nu(NH)_{carb}$, 2160 $\nu(C{\equiv}N)$, 1736 $\nu(C{=}O)_{carb}$, 1647 $\nu(C{=}O)_{benzoyl}$ 1595 $\nu(C{=}N)$. $^1H$ NMR (DMSO-$d_6$, $\delta$, ppm): 11.80 $(NH)_{Bz}$, 7.41, 7.86, 7.85 ($CH_{Bz}$, m, 3H), 7.60, 7.58, 7.4, 7.25 ($CH_{benzoyl}$, dd, 4H), 3.84 ($CH_3$, s, 3H), 3.22 (OH, s, MeOH), 2.55 ($CH_3$, m, MeOH). UV–Vis (DMF, $10^{-4}$, nm): 271, 320. Molar cond. (DMF, $10^{-3}$ M, $\Omega^{-1}$ $cm^2$ $mol^{-1}$): 46.10.

### Instruments

FT-IR spectra were recorded as potassium bromide pellets using a Jasco FT-IR 460 plus in the range of 4000–200 $cm^{-1}$. $^1H$ NMR spectrum was recorded at 300 MHz in DMSO-$d_6$ using Varian-Oxford Mercury VX-300 NMR. Elemental microanalysis was performed using Elementer Vario EL III. TG/DTA analysis was performed in $N_2$ atmosphere (20 ml $min^{-1}$) in a platinum crucible with a heating rate of 10 °C $min^{-1}$ using a Shimadzu DTG-60H simultaneous DTG/TG apparatus. Electronic spectra were scanned on a Shimdazu Lambda 4B spectrophotometer. A digital Jenway 4310 conductivity with a cell constant of 1.02 was used for the molar conductance study.

### DFT calculations

Quantum chemical calculations were performed using the Gaussian03 package [53]. Geometry optimization and

MEP maps of complexes **1–4** in the gas phase was carried out with DFT method using the hybrid B3LYP functional [54]. The LANL2DZ effective core potential basis set [16–18] was used for Pd atom, while 6-31G* was employed for the rest of atoms. The complexes were characterized as local minima through harmonic frequency analysis. Electronic transitions were calculated by TD-DFT [39]. The effect of solvent (DMSO) was performed using the default polarizable continuum model (PCM). Natural bond orbital (NBO) analysis was performed at the DFT/B3LYP/LANL2DZ level of theory.

## Biology

*In vitro evaluation of antimicrobial activity*

The antibacterial activity of compounds was tested on *Staphylococcus aureus* as a Gram-positive bacterium, and *Escherichia coli* as a Gram-negative bacterium according to a modified Kirby–Bauer disc diffusion method under standard conditions using Mueller–Hinton agar medium (tested for composition and pH), as previously reported [49, 55].

## Cytotoxicity assays

The anticancer activity was screened in vitro against *breast cancer* (MCF7), *colon carcinoma* (HCT) and *human hepatocarcinoma* ($HepG_2$) using Skehan et al. method [56]. The tumor cell line was maintained in the National Cancer Institute, Cairo, Egypt, by serial sub-culturing. Cells were plated in 96-multiwell plate ($5 \times 10^3$–$4 \times 10^4$ cells $well^{-1}$) for 24 h before treatment with various concentrations of the tested compounds (0, 5, 15, 25 and 50 $\mu g\ ml^{-1}$). RPMI-1640 medium (5 % fetal bovine serum and 2 mM L-glutamine) was used for culturing and maintenance of MCF7 cell lines [57]. Fixation of cells was performed by the addition of 10 % cold trichloroacetic acid. The different concentrations of the compounds under study were added to the cell monolayer triplicate wells were prepared for each individual dose. The monolayer cells were incubated with the compounds for 48 h at 37 °C and in 5 % $CO_2$ atmosphere. After 48 h, cells were fixed, washed, and stained with the protein-binding dye sulforhodamine B (SRB) [58]. Excess stain was washed with acetic acid and attached stain was recovered with tris–EDTA buffer. The optical density (OD) of each well was measured spectrophotometrically at 564 nm with an ELIZA microplate reader and the mean background absorbance was automatically subtracted and mean values of each drug concentration was calculated. The relation between surviving fraction and drug concentration was plotted to get the survival curve. The results were compared with a similar run of *cis-platin* as an antitumor compound.

## References


1. V. Rajendiran, M. Murali, E. Suresh, S. Sinha, K. Somasundaram, M. Palaniandavar, Dalton Trans. 148 (2008)
2. J. Mann, A. Baron, Y. Opoku-Boahen, E. Johansson, G. Parkinson, L.R. Kelland, S. Neidle, J. Med. Chem. **44**, 138 (2001)
3. D.I. Edwards, Biochem. Pharmacol. **35**, 53 (1986)
4. G.E. Adama, I.J. Strarford, Biochem. Pharmacol. **35**, 71 (1986)
5. D.C. Hodgkin, J. Kamper, M. Mackay, J. Pickworth, K.N. Trueblood, J.G. White, Nature **178**, 64 (1956)
6. S.J. Hsu, K.M. Hsu, M.K. Leong, I.J.B. Lin, Dalton Trans. 1924 (2008)
7. W. Xie, Y. Zhao, C. Li, S. Liu, Solid-State Electron. **51**, 1129 (2007)
8. Z. Ge, T. Hayakawa, S. Ando, M. Ueda, T. Akiike, H. Miyamoto, T. Kajita, M.A. Kakimoto, Chem. Mater. **20**, 2532 (2008)
9. G. Schwartz, K. Fehse, M. Pfeiffer, K. Walzer, K. Leo, Appl. Phys. Lett. **89**, 83509 (2006)
10. L. Li, G.J. Clarkson, Org. Lett. **9**, 497 (2007)
11. V. Rajendiran, M. Murali, E. Suresh, S. Sinha, K. Somasundaram, M. Palaniandavar, Dalton Trans. 2157 (2008)
12. D. Sperandio, A.R. Gangloff, J. Litvak, R. Goldsmith, J.M. Hataye, V.R. Wang, E.J. Shelton, K. Elrod, J.W. Janc, J.M. Clark, K. Rice, S. Weinheimer, K.S. Yeung, N.A. Meanwell, D. Hernandez, A.J. Staab, B.L. Venables, J.R. Spencer, Bioorg. Med. Chem. Lett. **12**, 3129 (2002)
13. E. Bouwmann, W.L. Driessen, J. Reedijk, Coord. Chem. Rev. **104**, 143 (1990)
14. M.A. Puja, T.D. Bharamgouda, N.D. Sathyanarayna, Trans. Met. Chem. **13**, 423 (1988)
15. G.D. Fallon, B. Moubaraki, K.S. Murray, A.M. van den Bergen, B.O. West, Polyhedron **12**, 1989 (1993)
16. N.T. Abdel-Ghani, A.M. Mansour, Inorg. Chim. Acta **373**, 249 (2011)
17. A.M. Mansour, Inorg. Chim. Acta **408**, 186 (2013)
18. N.T. Abdel-Ghani, M.F. Abo El-Ghar, A.M. Mansour, Spectrochim. Acta A **104**, 134 (2013)
19. H.C. Yao, M.M. Li, G.S. Yang, Z.J. Li, Y. Zhu, Inorg. Chim. Acta **360**, 3959 (2007)
20. L. Wei, J.W. Babich, W. Ouellette, J. Zubieta, Inorg. Chem. **45**, 3057 (2006)
21. M. Huang, P. Liu, J. Wang, Y. Chen, Z. Liu, Q. Liu, Inorg. Chem. Commun. **9**, 952 (2006)
22. C.K. Lee, K. M. Hsu, C.H. Tsai, C.K. Lai, I. J.B. Lin, Dalton Trans. 1120 (2004)
23. K. Isele, V. Broughton, C.J. Matthews, A.F. Williams, G. Bernardinelli, P. Franz, S. Decurtins, Dalton Trans. 3899 (2002)
24. A.E.M. Boelrijk, S.V. Khangulov, G.C. Dismukes, Inorg. Chem. **39**, 3009 (2000)
25. A. Patat, M.C. Perault, B. Vandel, Br. J. Clin. Pharmacol. **39**(1), 31 (1995)
26. M. Elissondo, L. Ceballos, M. Dopchiz, M.V. Andresiuk, L. Alvarez, S. Sanchez-Bruni, Parasitol. Res. **100**, 1003 (2007)
27. M. Elissondo, M. Dopchiz, L. Ceballos, L. Alvarez, S. Sanchez-Bruni, C. Lanusse, Parasitol. Res. **98**, 317 (2006)
28. A. Davis, Z.S. Pawlowski, H. Dixon, Bull. World Health Org. **25**, 235 (1986)
29. P. Reco, E. Hornus, J. Frejevus, P. Micheau, M.H. Bessieres, C. Roques, Bull Soc Fr Parasitol **3**, 115 (1984)
30. H. Bartikova, L. Skalova, J. Lamka, B. Szotakova, M. Varady, Helminthologia **47**(4), 269 (2010)
31. E. Hanser, H. Mehlhorn, D. Hoeben, K. Vlaminck, Parasitol. Res. **89**, 63 (2003)
32. S.P. Kan, T. Roy, Soc. Trop. Med. H **77**(5), 668 (1983)

33. S. Squires, M. Fisher, O. Gladstone, S. Rogerson, P. Martin, S. Martin, H. Lester, R. Sygall, N. Underwood, Vet. Parasitol. **185**, 352 (2012)
34. W. Baeyensl, F. Abdel, Fattah, P. De Moerloose. J. Pharm. Biomed. Anal. **3**(5), 397 (1985)
35. N. El-Enany, F. Belal, M. Rizk, Farmaco **58**(8), 613 (2003)
36. G. Dusi, V. Gamba, E. Faggionato, J. Pharm. Biomed. Anal. **38**, 375 (2005)
37. V. Cvilink, L. Skálová, B. Szotáková, J. Lamka, R. Kostiainen, R.A. Ketola, Anal. Bioanal. Chem. **391**, 337 (2008)
38. F.T. Martins, P.P. Neves, J. Ellena, G.E. Camí, E.V. Brusau, G.E. Narda, J. Pharm. Sci. **98**(7), 2336 (2009)
39. N.T. Abdel-Ghani, A.M. Mansour, J. Coord. Chem. **65**(5), 763 (2012)
40. N.F. Curtis, Y.M. Curtis, Inorg. Chem. **4**, 804 (1965)
41. B.P. Lever, E. Montovani, Can. J. Chem. **49**, 1957 (1971)
42. K. Nakamoto, *Infrared and Raman Spectra of Inorganic and Coordination Compounds, Part B: Applications in Coordination, Organometallic, and Bioinorganic Chemistry*, 6th edn. (Wiley, New Jersey, 2009)
43. N.T. Abdel-Ghani, A.M. Mansour, J. Mol. Struct. **991**, 108 (2011)
44. I. Lakomska, M. Barwiolek, E. Szlyk, Trans. Met. Chem. **32**, 70 (2007)
45. A. Bakalova, H. Varbanov, R. Buyukliev, G. Momekov, D. Ivanov, J. Therm. Anal. Calorim. **95**, 241 (2009)
46. N.T. Abdel Ghani, A.M. Mansour, Eur. J. Med. Chem. **47**, 399 (2012)
47. M. Krishnamurthy, P. Phaniraj, S.K. Dogra, J. Chem. Soc. Perkin Trans. II 1917 (1986)
48. V.I. Sokol, V.V. Davidov, M.A. Porai-Koshits, B.E. Zaitsev, M.V. Palishkin, G.V. Sheban, V.I. Pakhomov, S.S. Kukalenko, Izvestiya Akademii Nauk SSSR, Seriya Khimicheskaya **6**, 1306 (1988)
49. A.E. Reed, L.A. Curtiuss, F. Weinhold, Chem. Rev. **88**, 899 (1988)
50. A.M. Mansour, Polyhedron **78**, 10 (2014)
51. W.T. Shier, *Mammalian Cell Culture on $5 a Day: A Lab Manual of Low Cost Methods* (University of the Philippines, Los Banos, 1991), p. 64
52. A.M. Mansour, Spectrochim. Acta A **123**, 257 (2014)
53. A.M. Mansour, J. Coord. Chem. **67**(16), 2680 (2014)
54. M.J. Frisch, G.W. Trucks, H.B. Schlegel, G.E. Scuseria, M.A. Robb, J.R. Cheeseman, V.G. Zakrzewski, J.A. Montgomery, R.E. Stratmann, J.C. Burant, S. Dapprich, J.M. Millam, A.D. Daniels, K.N. Kudin, M.C. Strain, O. Farkas, J. Tomasi, V. Barone, M. Cossi, R. Cammi, B. Mennucci, C. Pomelli, C. Adamo, S. Clifford, J. Ochterski, G.A. Petersson, P.Y. Ayala, Q. Cui, K. Morokuma, D.K. Malick, A.D. Rabuck, K. Raghavachari, J.B. Foresman, J. Cioslowski, J.V. Ortiz, A.G. Baboul, B.B. Stefanov, G. Liu, A. Liashenko, P. Piskorz, I. Komaromi, R. Gomperts, R.L. Martin, D.J. Fox, T. Keith, M.A. Al-Laham, C.Y. Peng, A. Nanayakkara, C. Gonzalez, M. Challacombe, P.M.W. Gill, B.G. Johnson, W. Chen, M.W. Wong, J.L. Andres, M. Head-Gordon, E.S. Replogle, J.A. Pople, *GAUSSIAN 03 (Revision A.9)* (Gaussian, Inc., Pittsburgh, 2003)
55. A.M. Mansour, Dalton Trans. **43**, 15950 (2014)
56. P. Skehan, R. Storeng, J. Natl Cancer Inst. **42**, 1107 (1990)
57. C.M. Lozano, O. Cox, M.M. Muir, J.D. Morales, J.L. Rodríguez-Cabáin, P.E. Vivas-Mejfa, F.A. Gonzalez, Inorg. Chim. Acta **271**, 137 (1998)
58. National Committee for Clinical Laboratory Standards, NCCLS Approval Standard Document M2-A7, Vilanova, PA (2000)